

Laminar-turbulent transition reversal on blunt ogive body of revolution at hypersonic speeds

A. Vaganov, A. Noev*, V.Radchenko*, A.Skuratov* and A. Shustov***

**Central Aerohydrodynamic Institute (TsAGI)*

140180, Zhukovsky Str. 1, Zhukovsky, Russia

***Moscow Institute of Thermotechnics (MIT)*

123273, Berezovaya Al., 10, Moscow, Russia

Abstract

Influence of flow parameters and nose radius on laminar-turbulent transition location is under investigation. Model used was ogive-conical body of revolution having half angle about 9° . Experiments were conducted in shock tunnel at Mach number 5. Transition location was diagnosed by heat transfer rate distribution determined with aid of luminescent temperature converters. It is shown that transition reversal can occur either a) in absence of turbulent wedges or b) at constant level of freestream disturbances. Both increasing and decreasing branches of $Re_{\infty,t}(Re_{\infty,R})$ dependency were observed at constant nose radius while varying unit Reynolds number only.

1. Introduction

Phenomenon of laminar-turbulent transition reversal was found about 50 years ago during experiments with blunt cones in hypersonic wind tunnel [1]. The thing is increasing nose bluntness radius R leads to downstream shift of transition onset location, however it happens only until some critical value of R (or Reynolds number $Re_{\infty,R,crit}$) is reached. Afterwards reversal tendency is observed, at that rather strong; transition point moves to the nose. Existence of the phenomenon is confirmed by later wind tunnel experiments [2-7, 26] on blunt cones and plates. As of today, nature of the phenomenon is unclear. Linear stability theory calculations show that at moderate bluntness transition location corresponds to growth of 2nd Mack mode [15,9]. However transition on reversal regime cannot be described by simple growth of 1st or 2nd mode [20,9].

In [7] extensive experimental data are classified by relative locations of transition onset and absorption of entropy layer by boundary layer. Three transition regimes were distinguished: near absorption point (and further downstream), before absorption point and in the initial portion of entropy layer. Experimental data pretty good fit this concept, which was later numerically confirmed in [5]. Despite of this, mechanism of transition onset upstream movement on 2nd and 3rd regimes remained unclear

Author of [23] suggested similar classification using parameter x_{EW} . It is distance from nosetip to the point on blunt cone where pressure becomes equal to pressure on corresponding sharp cone. This parameter is less ambiguous than swallowing length. In [2] it is suggested that the character point is where boundary layer edge Mach number becomes one less than sharp cone Mach number. Both correlations describe experimental data well.

Parameter that generalizes $Re_{\infty,R}$: $K = (Re_{\infty,R})^{0.5} \times M_\infty^2 \times \sin(\theta)$, (θ – cone half angle) was suggested in [4]. Experimental data in range $M_\infty=5-12$, $\theta=5-10^\circ$, $R=0.064-63\text{mm}$ are described by universal dependency $Re_{\infty,t}(K)$ pretty good (fig. 4). Similar to $Re_{\infty,t}(Re_{\infty,R})$ dependency, $Re_{\infty,t}(K)$ dependency consists of increasing and decreasing parts.

In contrast in [26] it is shown that no reversal is observed when using $Re_{\infty,t}^{**}(Re_{\infty,R})$ coordinates. However this paper has some issues for example whether we talk about transition onset or end, relatively low Mach numbers and nose bluntness so on.

In [7] to determine role of positive pressure gradient behind blunt nosetip two models were used: conical and ogive. Ogive model were designed such that pressure gradient was negative on whole model length. Surprisingly, on this model transition happened a little earlier than on the conical one in similar flow. One of possible reasons of this could be different surface roughness.

In [13] high-level pulsations was found inside entropy layer. It was supposed that they are growing inside boundary layer leading to transition. Stability calculations in [21] agreed that near swallowing point these pulsations

can resonate with boundary layer modes of instability. Experiments [27] partially agreed with this. Calculations [24] revealed some mode of entropy layer instability with dimensionless frequency close to [13].

In [5] at relatively high value of $R=50.8\text{mm}$ increasing part of $Re_{\infty,t}(Re_{\infty,R})$ dependency was observed. At that for lower R values typical reversal is observed as in other papers. In other words, at large enough R decreasing part of $Re_{\infty,t}(Re_{\infty,R})$ dependency becomes increasing again (see fig. 4). Though this conclusion needs additional verification, such a phenomenon can be of much interest.

Numerical modeling of experiments using linear stability theory was performed in [5,7-9,20]. On the increasing part of $Re_{\infty,t}(Re_{\infty,R})$ curve experiments agree well with calculations of 2nd Mack mode instability[15]. N-factors calculated for both 1st and 2nd modes on decreasing part turn out to be too small for them to cause transition [5, 9, 20, 27]. Probably reason of this should lie among factors not accounted for in simulations namely: model surface roughness [19,28], increase of wind tunnel freestream disturbances level when increasing Reynolds number leading to bypass regime of transition [8], nonlinear grows of disturbances [20], so on.

Parameter $Re_{\infty,R} = Re_{\infty,1} \times R$ is connected with at once three different factors potentially influencing transition location: nose radius, freestream disturbances level (for account of $Re_{\infty,1}$), and surface roughness height relative to boundary layer thickness. It seems reasonable to consider these factors separately.

Let us consider in detail question about surface roughness. It can lead to transition by two ways: through turbulent wedges originating from discrete high enough surface irregularities and steep generation of disturbances due to distributed roughness. In [28] it is argued that namely last way (so called “transient growth”) is transition mechanism on reversal regime. However, that paper deals only with transition occurred on rough nosetip near sonic line. Whereas massive reversal data, including pioneer one ([1-3, 5], present data) show transition occurred far downstream of sonic line still through unknown mechanism. What concerns turbulent wedges, in [6] it is shown that their formation can lead to transition movement to the nose thus producing wedges-induced reversal. In capacity of significant source of surface irregularities, we should note the joint between changeable nosetip and main model part [7].

Known to the authors numerical simulations of experiments do not account for roughness. To sorry in many reversal observations it is impossible to answer whether there existed turbulent wedges. It is due to measurements were carried out using discrete sensors. Exceptions are [5, 6, 10] where panoramic measurement technique was used (as in present work). In [6] reversal was namely due to wedges originating near nosetip. Data [10] obtained in the same shock tunnel, same inflow, same measurement technique and geometrically close model shape as [6]. No reversal and no wedges were observed probably due to significantly lower model roughness. In [5] both sensors and panoramic measurements were used but data presented demonstrates absence of wedges only in part of tunnel runs done.

Let us consider in detail question about incoming flow disturbances. Increasing $Re_{\infty,R}$ for account of $Re_{\infty,1}$ (in turn for account of pressure) means increasing level of inflow acoustic pulsations [14]. After reaching some critical amplitude these pulsations can trigger “bypass” transition scenario [22]. This scenario is not described by linear theory. In [8] this scenario is suggested as possible reason of reversal absence in calculations. However data obtained in [4] clearly indicate that reversal can be observed at **fixed** $Re_{\infty,1}$ (therefore fixed flow disturbances level) and increased R . In this case, reversal still could be triggered by bypass scenario due to possible increase of boundary layer sensitivity to bypass with increasing radius. Unfortunately, no flight [25] or ballistic range [29] data on smooth-body reversal are available. This is often due to ablation or too small $Re_{\infty,R}$ values realized.

2. UT-1M shock tunnel

Experiments were spent in TsAGI wind tunnel UT-1M. It is shock tunnel running by Ludwig scheme [16] (fig. 1).

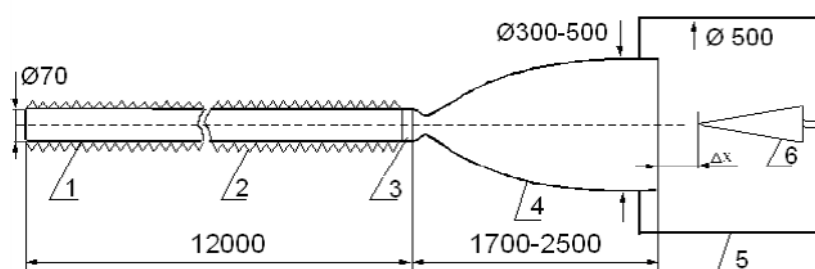


Figure 1 : Scheme of UT-1M facility.

1–High pressure channel, 2–electric heater unit, 3–diaphragm section, 4–nozzle, 5–test section, 6–model.

Before run gas to the right from metal diaphragm is pumped out to low pressure – 100 Pa while gas to the left from diaphragm is pumped in to high pressure (up to 10 MPa). Due to pressure delta diaphragm is destroyed and gas flows into test section. Duration of stationary flow is only 35-40 msec but it is enough for establishing of shock waves and boundary layer (at least outside of separation regions). This is verified by high-speed shadowgraphs and pressure and temperature sensors placed on nozzle side. In current work nozzle was used that provides test section flow at Mach number $M_\infty=5$ with exit diameter 300 mm. More detailed facility description can be found in [11, 12].

3. Measurement technique and model

Investigation of model external surface heating was carried out using panoramic optical instrumentation – luminescent temperature converters. Its working principle is as follows. Model surface is sprayed with thin layer of special coating. Intensity of its luminescence under exciting radiation depends only on its temperature, coating thickness and is directly proportional to intensity of exciting radiation intensity. Distribution of radiation intensity over model surface is registered with digital camera before and during run. Using coating calibration curve the intensity is recalculated to temperature. Using approximate analytical solution of inverse problem for heat conduction equation as well as coating thermophysical properties and time delta temperature delta is recalculated to dimensionless heat flux – Stanton number $St = q / (T_r - T_{in}) \rho_\infty V_\infty C_p$ [17]. Here q – heat flux density at given point on model surface (W/cm^2), ρ_∞ , V_∞ , C_p – respectively density, velocity and heat capacity of incoming flow, T_r – recovery temperature (assumed $T_r = T_0$), T_{in} – initial surface temperature.

To enhance measurement accuracy so called binary luminescent temperature converters were used in present work. It contains two luminophores: active and base one. Active one reacts to temperature unlike base one which radiates directly proportional to excitation. Both are excited with same wavelength but radiate in different spectral regions, which is needed to separate registration of two images. If intensities of active and base luminophores are registered simultaneously then measurement result does not depend on exciting intensity change caused either model vibration or instability of source. In-detail description of measurement technique and its errors can be found in [12,18].

For this methodology of heat flux density to model construction determination to work properly model surface should have thermophysical properties close to these of coating. AG-4 material meets this requirement so it was used. Before experiment model was coated with paint EP-140 based on epoxy resin with addition of zinc dioxide to level optical background of AG-4 material. To reduce surface roughness model was polished both before and with special care after coating with luminescent paint.

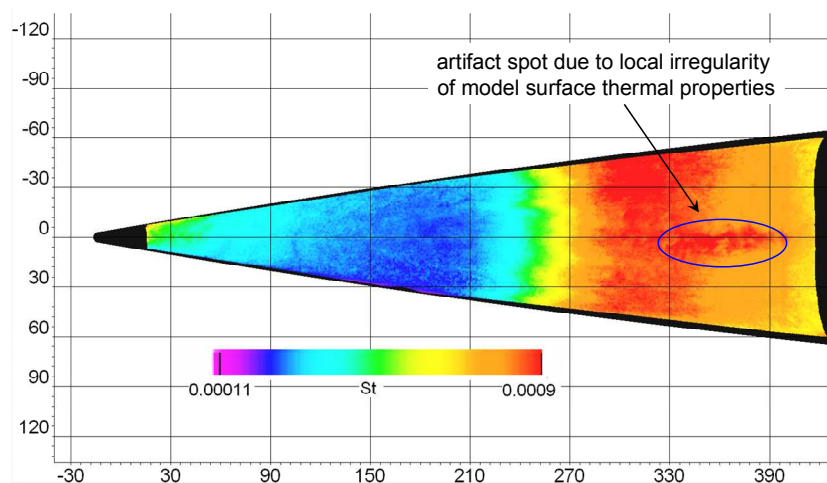


Figure 2 : Example of Stanton number distribution along model surface obtained by the method used. Flow direction is left to right. Dimensions are in mm. Run number 5312, $Re_{\infty,R} = 1.03 \times 10^5$, $R=3mm$.

Model presented ogive body 440 mm length with half-angle about 9° and $L=440$ mm length. Material of its main part is described above. Changeable aluminum nosetips of radius $R=1, 2, 3$ and 7 mm were used to vary nose bluntness. Geometrically nosetip consisted of sphere segment smoothly connected to conical part. The conical part in turn smoothly connected with main ogive part of the model. The lengths of $R=7$ and 1 mm nosetips were about 9 and 36 mm respectively. Model shape is depicted on fig. 2. Experiments were carried out at zero incidence.

Coating temperature change through test was increased negligible and remained close to initial temperature (before run): $T_w \approx 285-290$ K. Wall-to-total temperature ratio $T_w/T_0 \approx 0.55$.

Fig. 2 shows example of Stanton number distribution along model surface obtained by the method used.

4. Method of transition location determination

Transition location and end diagnosed by Stanton number distribution along some model generatrix. In case of absence of turbulent wedges, as it was in most runs done the choice of the particular generatrix had little effect on Stanton number distribution as well as transition location (see fig. 2).

Let us consider more general case when microroughness generates turbulent wedge. Figure 3.a) shows panoramic distribution of Stanton number in this case. Figure 3.b) shows Stanton number distributions along two generatrices: one goes through the wedge while another lies outside of its influence. Point of onset and end of the growth in the distribution correspond to transition onset and end respectively. Stanton number values lying in laminar and turbulent regions agree well for the generatrices. Transition onset x-coordinate on first generatrix is about 2 times lower than that on second generatrix. As for transition end it is about 2.2 times. This illustrates the need to carefully monitor wedges emerging in transition experiments.

Within present work, transition location for runs with wedges always was determined considering generatrix that located outside of its influence. Such a generatrix did exist for all runs done. Thus, influence of local microroughnesses is eliminated.

In present work when calculating transition Reynolds number, coordinate of transition onset location x_t was counted from stagnation point along model axis.

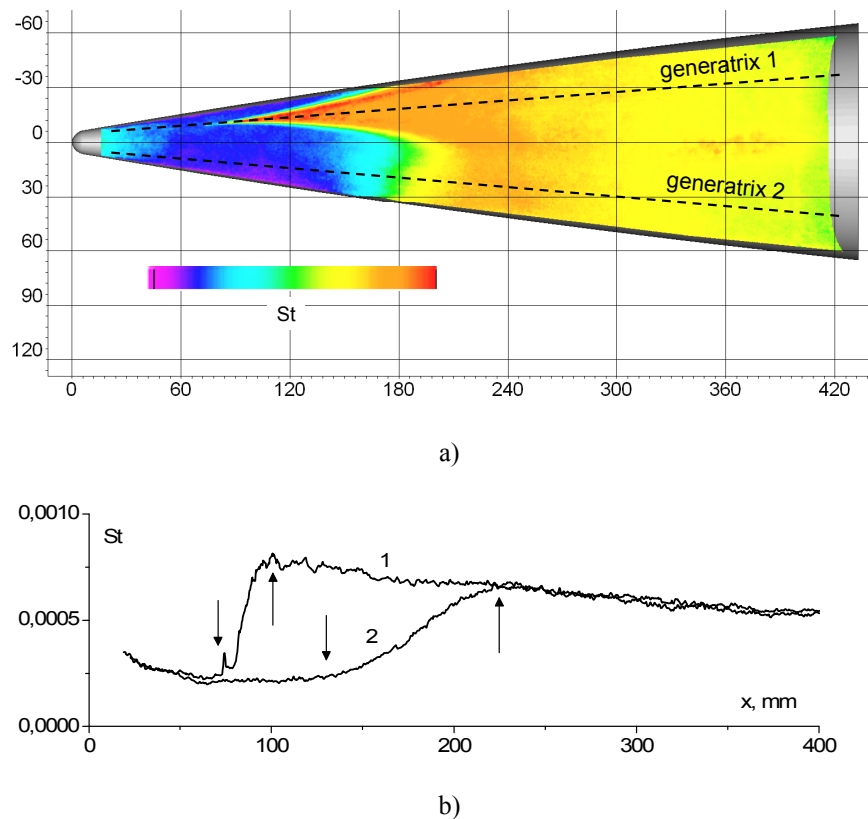


Figure 3 : Example of transition location determination by longitudinal Stanton number distribution. Run number 5308, $Re_{\infty,R} = 4.79 \times 10^5$, $R=7\text{mm}$. Down and up arrows – correspondingly onset and end of transition for two generatrices.

5. Results

Fig. 4.a) shows reversal data from various experiments and correlation using parameter K (figure taken from [4]). Fig. 4.b) shows present data and data [5] in similar manner. There is satisfactory agreement. Need to note mentioned in introduction region of secondary growth in $Re_{\infty,t}(Re_{\infty,R})$ dependency after reversal at relatively large R (curve 3). Fig. 5 shows present data replotted to demonstrate reversal phenomenon at two ways of $Re_{\infty,R}=Re_{\infty,1} \times R$ growth: R growth at fixed $Re_{\infty,1}$ (curve 1) and vice-versa $Re_{\infty,1}$ growth at fixed R (curve 2).

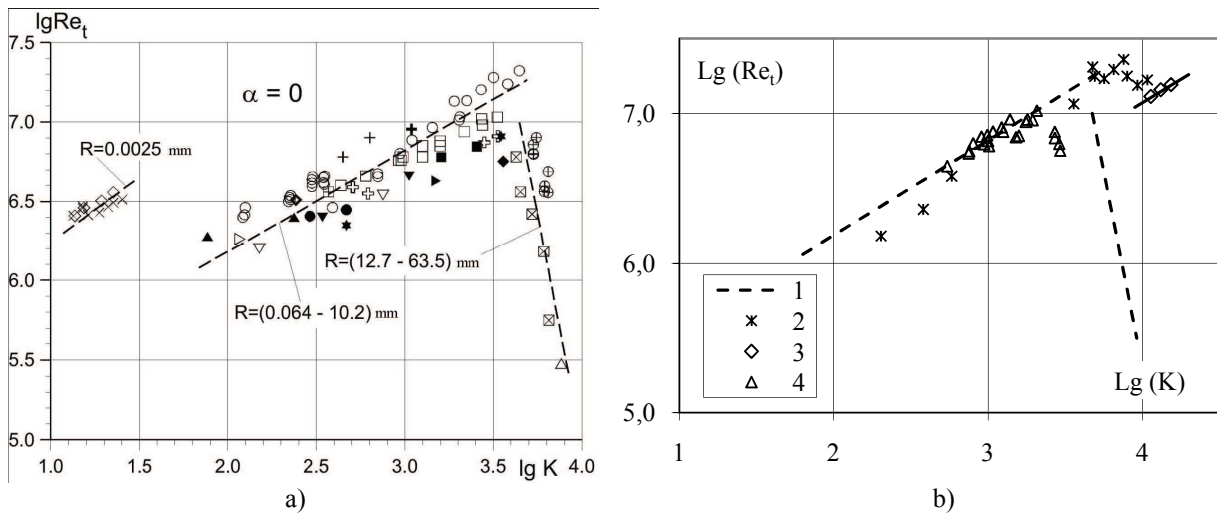


Figure 4 : a) Correlation of data on blunt cone transition [4]. Data taken from [3,4,23,30-35]. $M_\infty=5-12$, $\theta=5-10^\circ$, $R=0.064-63\text{mm}$. $K = (\text{Re}_{\infty,R})^{0.5} \times M_\infty^2 \times \text{Sin}(\theta)$ (θ – cone half angle).
 b) 1 – correlation [4]; 2 – [5] ($\theta=7^\circ$, $M_\infty=10$); 3 – [5], $R=50.8\text{mm}$; 4 - present data ($\theta \approx 9^\circ$, $M_\infty=5$).

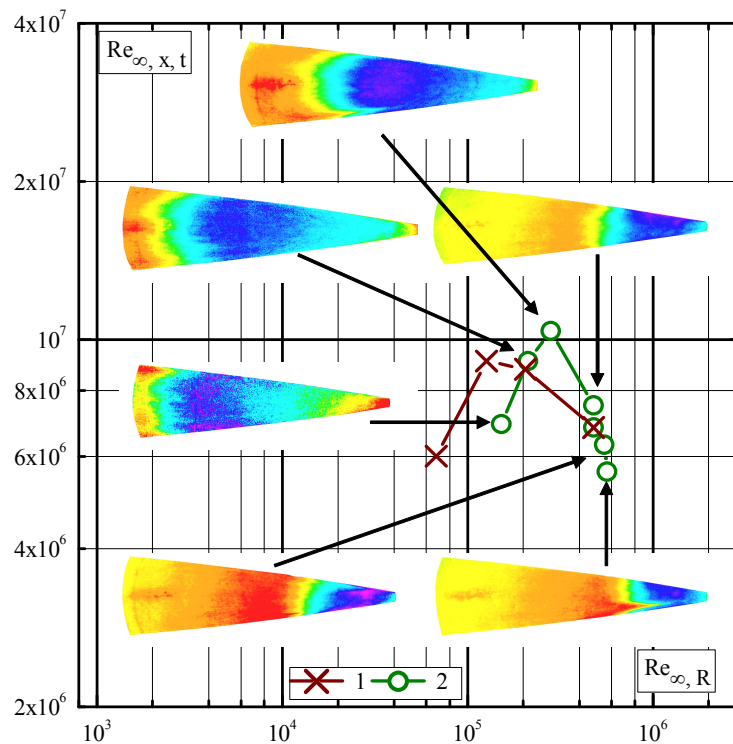


Figure 5 : Reversal at:

1 – $R=1-7\text{mm}$, $\text{Re}_{\infty,1}=6.6 \times 10^7 \pm 4\% \approx \text{const}$; 2 – $R=7\text{mm}=\text{const}$, $\text{Re}_{\infty,1} \approx 2.2-8.0 \times 10^7$.

Let us consider curve 1 fig. 5. Authors of [8] as hypothetical cause of reversal rightly mention growth of freestream disturbances when increasing $\text{Re}_{\infty,1}$. It could lead to bypassing linear stage of transition thus explaining discrepancies between linear theory and experiment concerning transition onset location. $\text{Re}_{\infty,1}$ and freestream disturbances is almost constant on curve 1. Still reversal is here. Similar effect presented earlier in [4]. Therefore, freestream disturbances growth is not the reversal reason at least in present case. Need to mention that this does not eliminate

possibility that “bypass”-regime realized here. It still could realize due to possible growth of boundary layer sensitivity at growing R and constant external disturbances level.

Let us consider curve 2 fig. 5. In all known to authors reversal experiments following fact is observed. At fixed R , the $Re_{\infty,t}$ ($Re_{\infty,R}$) dependency is always monotone – increasing (at small R) or decreasing (at large R). While the dependency seems to be common line for all radiuses. It would seem that at some intermediate R one should observe both increasing and decreasing parts but this did not happen. This strange fact probably is due to just too large step for R and too narrow $Re_{\infty,1}$ range since it do happen on curve 2 fig. 5.

In principle, there is arbitrariness when quantitatively determining transition location. One can count x_t coordinate along cone axis or generatrix; from location of stagnation point (different for different R), virtual sharp cone nose (same for different R) or sphere-cone junction so on. Presence of reversal on curve 2 at fixed R implies that it would exist using any method. Original panoramic St distributions corresponding to points of curve 2 are shown on fig. 5. For each picture color scale is chosen so that to clearly demonstrate transition onset location. It is located just after the purple region corresponding to local St minimum. One can see turbulent wedges in some runs, particularly at maximum $Re_{\infty,R}$ value. Note that there is no wedge on the distributions corresponding to the first two points on decreasing branch of the curve. This directly demonstrates that at least in present experiments reversal has no concern to local surface microroughness.

5. Conclusions

Due to author’s knowledge, for the first time both increasing and decreasing branches of $Re_{\infty,t}$ ($Re_{\infty,R}$) dependency were observed at constant nose radius while varying unit Reynolds number only.

It is shown that during present experiments transition reversal had no concern to turbulent wedges produced by local surface microroughness as well as to growth of freestream disturbances level in case of wind tunnel pressure growth. This thickens a range of factors potentially responsible for reversal phenomenon.

6. Acknowledgments

Authors want to thank N.B. Larin and I.V. Struminskaya for taking part in conduction and processing of the experiments. The work was supported by Russian Foundation of Fundamental Research, project 16-01-00743.

References

- [1] K. Stetson, G. Rushton. 1967. Shock tunnel investigation of boundary-layer transition at $M=5.5$. *AIAA J.* 5:899-906.
- [2] J. Softley. 1969. Boundary layer transition on hypersonic blunt, slender cones. *AIAA Paper.* 705.
- [3] J. Muir, A. Trujillo. 1972. Experimental investigation of the effects of nose bluntness, free-stream unit Reynolds number and angle of attack on cone boundary layer transition at a Mach number of 6. *AIAA Paper.* 216.
- [4] V. Brazhko, A. Vaganov, N. Kovaleva, N. Kolina, I. Lipatov. 2009. Experimental and numerical investigations of boundary layer transition on blunted cones at supersonic flow. *TsAGI Sci. J.* 3:1-11.
- [5] E. Marineau, C. Moraru, D. Lewis, J. Norris, J. Lafferty, R. Wagnild, J. Smith. 2014. Mach 10 boundary-layer transition experiments on sharp and blunted cones. *AIAA Paper.* 3108.
- [6] E. Aleksandrova, A. Novikov, S. Utyuzhnikov, A. Fedorov. 2014. Experimental investigation of laminar-turbulent transition on blunted cone. *J. App. Mech. Tech. Phys.* 3:5-16.
- [7] K. Stetson. 1983. Nosetip bluntness effects on cone frustum boundary layer transition in hypersonic flow. *AIAA Paper.* 1763.
- [8] J. Lei, X. Zhong. 2012. Linear stability analysis of nose bluntness effects on hypersonic boundary layer transition. *J. Spacecraft and Rockets.* 1:24-37.
- [9] J. Jewell, R. Kimmel. 2016. Boundary layer stability analysis for Stetson’s Mach 6 blunt cone experiments. *AIAA Paper.* 598.
- [10] A. Vaganov, A. Noev, V. Plyashechnik, V. Radchenko, A. Skuratov, A. Shustov. 2016. Laminar-turbulent transition on a blunted ogive-conical body at hypersonic speeds. *AIP Conference Proceedings.* 1770. 030049.
- [11] V. Borovoy, V. Mosharov, A. Noev, V. Radchenko. 2009. Laminar-turbulent flow over wedges mounted on sharp and blunt plates. *Fluid Dynamics.* 3:382-396.

- [12] V. Borovoy, V. Mosharov, A. Noev, V. Radchenko. 2012. Temperature sensitive paint application for investigation of boundary layer transition in short-duration wind tunnels. In: *Progress in Flight Physics*. 15-24.
- [13] K. Stetson, E. Thompson, J. Donaldson L.G. Siler. 1984. Laminar boundary layer stability experiments on a cone at mach 8, part 2: blunt cone. *AIAA Paper*. 6.
- [14] S. Pate. 1977. Dominance of radiated aerodynamic noise on boundary layer transition in supersonic-hypersonic wind tunnels. *AEDC TR*. 107. See also: S. Pate. 1980. Effect of wind tunnel disturbances on boundary-layer transition with emphasis on radiated noise: a review. *AIAA paper*. 431.
- [15] L. Mack. 1975. Linear stability theory and the problem of supersonic boundary-layer transition. *AIAA J*. 3:278-289.
- [16] A. Kharitonov. 2005. Technique and methods of aerophysical experiment. Part 1. Wind tunnels and gasdynamic facilities. NGTU. Novosibirsk. 220p. [in Russian]
- [17] V. Borovoy. 1983. Gas flow and heat transfer in zones of interaction between shock waves and boundary layer. Mashinostroenie. Moscow. 142p. [in Russian]
- [18] V. Mosharov. 2009. Luminescent methods for investigating surface gas flows (review). *Instr. and Exp. Tech*. 1:5-18.
- [19] S. Schneider. 2008. Summary of hypersonic boundary-layer transition experiments on blunt bodies with roughness. *J. Spacecraft and Rockets*. 6:1090-1105.
- [20] I. Rosenboom, S. Hein, U. Dallman. 1999. Influence of nose bluntness on boundary-layer instabilities in hypersonic cone flows. *AIAA paper*. 3591.
- [21] A. V. Fedorov. 1990. Instability of the entropy layer on a blunt plate in supersonic gas flow. *J. App. Mech. Tech. Phys*. 5:722-728.
- [22] M. Morkovin, E. Reshotko, T. Herbert. 1994. Transition in open flow systems — a reassessment. *Bull. Am. Phys. Soc*. 9:1882.
- [23] L. Ericsson. 1988. Effect of nose bluntness and cone angle on slender-vehicle transition. *AIAA J*. 10:1168-1174.
- [24] G. Dietz, S. Hein. 1999. Entropy-layer instabilities over a blunted flat plate in supersonic flow. *Phys. Fluids*. 1:7-9.
- [25] S. Schneider. 1999. Flight data for boundary-layer transition at hypersonic and supersonic speeds. *J. Spacecraft and Rockets*. 1:8-20.
- [26] V. Lebiga. 2014. The boundary layer transition at supersonic velocities. *J. App. Math. Mech*. 2:114-120.
- [27] A. Maslov, A. Shilyuk, D. Bountin, A. Sidorenko. 2006. Mach 6 Boundary-Layer Stability Experiments on Sharp and Blunted Cones. *J. Spacecraft and Rockets*. 1:71-76.
- [28] E. Reshotko. 2008. Roughness-induced transition, experiment and modeling. *AIAA paper*. 4294.
- [29] D. Reda, M. Wilder, D. Prabhu. 2012. Transition experiments on large bluntness cones with distributed roughness in hypersonic flight. *AIAA paper*. 446.
- [30] N. Kolina, Yu. Kolochinsky, A. Yushin. 1985. The influence of entropy layer absorption on heat exchange at supersonic flow over a circular cone. *TsAGI Sci. J*. 3:21-28. [in Russian]
- [31] N. Davydova, A. Yushin. 1973. Experimental investigation of the influence of angle of attack on the laminar-turbulent transition of the boundary layer at the circular cone overflow. *TsAGI Sci. J*. 2:45-53. [in Russian]
- [32] R. Davlet-Kildeev. 1977. Investigation of the boundary layer transition on the cone, streamlined by hypersonic gas flow at various angles of attack. *TsAGI trans*. 1881. [in Russian]
- [33] G. Widhopf, R. Hall. 1972. Transitional and turbulent heat-transfer measurements on a yawed blunt conical nose tip. *AIAA J*. 10:1318-1325.
- [34] T. Horvath, S. Berry, H. Hamilton. 2001. Qualitative assessment of the acoustic disturbance environment in the NASA LaRC 20-inch Mach 6 wind tunnel. In: 95th *Supersonic Tunnel Association International Meeting*.
- [35] T. Horvath, S. Berry, B. Hollis, C.-L. Chang, B. Singer. 2002. Boundary layer transition on slender cones in conventional and low-disturbance Mach 6 wind tunnels. *AIAA Paper*. 2743.